Title
Frontocerebellar gray matter plasticity in alcohol use disorder linked to abstinence

Authors
Muller, Angela M
Meyerhoff, Dieter J

Publication Date
2021

DOI
10.1016/j.nicl.2021.102788

Peer reviewed

NeuroImage: Clinical 32 (2021) 102788

Contents lists available at ScienceDirect

NeuroImage: Clinical

journal homepage: www.elsevier.com/locate/ynicl

Frontocerebellar gray matter plasticity in alcohol use disorder linked to abstinence

Angela M. Muller *, Dieter J. Meyerhoff

Department of Radiology and Biomedical Imaging, University of California San Francisco, San Francisco, USA
VA Advanced Imaging Research Center (VAARC), San Francisco VA Medical Center, San Francisco, CA, USA

ARTICLE INFO

Keywords:
Subcircuits
Default-mode network
Executive-control network
Salience network
Cerebellum
Longitudinal
Negative strength
Profile similarity index

ABSTRACT

Alcohol use disorder (AUD) is associated with brain-wide gray matter (GM) reduction, but the frontocerebellar circuit seems specifically affected by chronic alcohol consumption. T1 weighted MRI data from 38 AUD patients at one month of sobriety and three months later and from 25 controls were analyzed using voxel-based morphometry (VBM) and a graph theory approach (GTA). We investigated the degree to which the frontocerebellar circuit's integration within the brain's GM network architecture was altered by AUD-related GM volume loss. The VBM analyses did not reveal significant GM volume differences between relapsers and abstainers at either timepoint, but future relapsers at both timepoints had significantly less GM than controls in the frontocerebellar circuit. Abstainers, who at baseline also showed the most pronounced GM loss in the thalamus, showed a significant circuit-wide GM increase with inter-scan abstinence. The post-hoc GTAs revealed a persistent diffuse global atrophy in both AUD groups at follow-up relative to controls and different recovery patterns in the two AUD groups. Our findings suggest that future relapsers do not just present with a more severe expression of the same AUD consequences than abstainers, but that AUD affects the frontocerebellar circuit differently in relapsers and abstainers.

1. Introduction

Chronic alcohol abuse is associated with widespread gray matter (GM) atrophy across the entire brain as observed in region-of-interest and whole brain voxel-wise magnetic resonance imaging approaches (Cardenas et al., 2007; Chanraud et al., 2007; Chye et al., 2020; Demirakca et al., 2011; Grodin et al., 2013; Li et al., 2019; Mackey et al., 2019; Mechtcheriakov et al., 2007; Navarri et al., 2020; Pandey et al., 2018; Pitel et al, 2015; Ritz et al., 2016; Sullivan et al., 2003; Thayer et al., 2016; Xiao et al., 2015; Yang et al., 2016). However, not all brain regions commonly showing GM atrophy in association with long-term chronic alcohol consumption are specific for alcohol only. For example, GM atrophy in brain regions such as the medial orbitofrontal cortex, insula, middle temporal, and supramarginal gyri, hippocampus, amygdala, and nucleus accumbens (Mackey et al., 2019; Navarri et al., 2020) has also frequently been observed in other substance abuse disorders. In contrast, GM damage in other brain regions such as those belonging to the frontocerebellar circuit, in which the thalamus plays a central role, seems to be predominant for alcohol use disorder (AUD) (Le Berre et al., 2014; Pitel et al., 2015; Ritz et al., 2016; Sullivan et al., 2003; Zahr et al., 2017). The frontocerebellar circuit is implicated in a range of cognitive functions and behaviors such as executive functions, learning, memory, language but also postural stability and gross- and fine-motor functions (Chanraud et al, 2007; Chanraud-Guillermo et al., 2009; Sullivan and Pfefferbaum, 2005). Its involvement in cognition and behavior was also supported by fMRI resting-state connectivity analyses in healthy controls (Buckner et al., 2011; Habas et al., 2009; Krienen and Buckner, 2009). These studies have shown that the frontocerebellar circuit can be further divided in several distinct subcircuits, which correspond to well-established intrinsic connectivity networks such as the executive control network (ECN), default mode network (DMN), salience network (SAL), dorsal attention network, and sensorimotor network (SMN). Disruptions of these subcircuits are thought to be major contributors to behavior and cognition in AUD (Zahr et al., 2010; Sullivan and Pfefferbaum, 2005; Zhang and Volkow, 2019; Zahr et al., 2017).

Longitudinal neuroimaging studies paint a heterogeneous picture for GM recovery during abstinence from alcohol in treatment seekers that,

* Corresponding author at: Department of Radiology and Biomedical Imaging, VA Advanced Imaging Research Center, San Francisco VA Medical Center, 4150 Clement Street, Building 13, San Francisco, CA 94121, USA.
E-mail address: angela.muller@ucsf.edu (A.M. Muller).

https://doi.org/10.1016/j.nicl.2021.102788
Received 18 May 2021; Received in revised form 8 August 2021; Accepted 10 August 2021
Available online 13 August 2021

among other factors, depends on the level of GM deficits before treatment and duration of successful sobriety. Abstinence from alcohol as short as two weeks (Bach et al., 2020; van Eijk et al., 2013) has been associated with significant GM recovery (Cardenas et al., 2007; Segobin et al., 2014; Zou et al., 2018). Furthermore, treatment seeking AUD patients with faster GM recovery have a better chance of remaining abstinent for a longer time than those with slower recovery (Cardenas et al., 2007). Likewise, AUD patients with less GM atrophy early in treatment seem to have a better chance of successful abstinence than those with more severe atrophy (Durazzo et al., 2017), and the degree of prefrontal brain volume loss and recovery within the first month of abstinence has been shown to be associated with relapse in AUD treatment seekers (Durazzo and Meyerhoff, 2020). Therefore, the degree of GM atrophy in regions vulnerable to the specific effects of alcohol - such as the frontocerebellar circuit - early in treatment and their potential for recovery during treatment may be important indicators that distinguish AUD patients who succeed to stay sober from those who may need additional support to achieve the same goal.

One aim of this analysis was to follow-up on our previous findings in recovering treatment seekers with AUD (Cardenas et al., 2007; Durazzo and Meyerhoff, 2020) by investigating if abstainers had greater GM recovery in brain regions belonging to the frontocerebellar circuit than relapsers. Using a purely data-driven method at the voxel-level (Voxel Based Morphometry (VBM)) for the brain's GM including cortical and subcortical regions as well as cerebellum, we wanted to know specifically (a) if GM reduction in the frontocerebellar circuit can differentiate between future relapsers and future abstainers in a sample of 38 AUD patients at one month into treatment when they all were still abstinent, and (b) how these early GM differences related to both GM differences and their changes three months later when some of the AUD patients had relapsed. In a previous morphometric study of a similar patient cohort using graph theory analysis (GTA) (Mueller and Meyerhoff, 2021), we observed that regions with AUD-related local GM atrophy do not represent GM alterations that are independent of each other but can be better understood as a network of co-altered brain regions. Furthermore, brain regions with AUD-related atrophy also have the potential to alter how not affected neighboring and remote regions are integrated within the GM network organization of the entire brain (Mueller and Meyerhoff, 2021). These earlier observations are consistent with the "network degeneration hypothesis" (Cauda et al., 2020; Liloia et al., 2021; Seeley et al., 2009), which is based on physiological evidence of synchronous neuronal firing that supports network-based synaptogenesis (Seeley et al., 2009) and on the observation that atrophy patterns in neurological and psychiatric conditions frequently resemble distinct intrinsic connectivity networks found in healthy controls (Cauda et al., 2020; Liloia et al., 2021; Seeley et al., 2009). Furthermore, intrinsic connectivity networks are not isolated entities within the brain but are characterized by finetuned and dynamic interactions with each other (Wig, 2017). Atrophy-related functional disturbance in one network therefore has the potential to affect how this network functionally interacts with the brain's other intrinsic connectivity networks (Hoffstaedter et al., 2015; Mueller and Weiner, 2017; Shafiei et al., 2020). Neuronal firing patterns altered in this way then have the potential to lead to corresponding changes in synaptogenesis or dendritic spine density, both of which can be picked up by VBM (Keifer et al., 2015). The findings of our previous publication using GTA and PSI in the context of predefined ROIs (Mueller and Meyerhoff, 2021) in combination with the new VBM findings of our study's first specific aim, motivated the second aim of the study: using the same GTA approach as Mueller and Meyerhoff (2021) in a post-hoc analysis to investigate the degree to which the VBM-detected (i.e., voxel-wise) local GM atrophy affected the integration of four behaviorally relevant frontocerebellar subcircuits within the GM network organization of the entire brain; those subcircuits are the DMN, ECN, SAL, and SMN. Given the distinctly different atrophy and recovery patterns already described in relapsers and abstainers, we hypothesized that disentangling the role of these four frontocerebellar subcircuits in the two AUD groups at baseline and follow-up would help to gain additional knowledge into which gray matter features may promote abstinence or may predict relapse.

2. Methods

2.1. Participants

Longitudinal T1 weighted 3T MRI data from 38 AUD patients and 25 healthy non-drinking/light drinking controls were used for this study. The AUD participants were recruited from outpatient treatment clinics in San Francisco, CA in the context of an ongoing study on polysubstance use disorders, and they belong to a group of individuals with alcohol use disorder diagnoses only. All AUD participants came for the first MRI examination approximately one month into abstinence (=baseline) and returned for their follow-up appointment approximately three months later (=follow-up). The drinking status of the AUD individuals at follow-up determined their group allocation for the purpose of this analysis: 23 AUD individuals started consuming alcohol again during the three-months interval and were classified as relapsers, whereas 15 AUD individuals stayed successfully sober during the three-months interval and were classified as abstainers. The controls were recruited from the local community, and all were scanned twice with identical MRI sequences and at the same time interval as AUD participants. However, because only 13 controls from the polysubstance use disorder study had a complete data set with baseline and fellow-up at the time of analysis, the control group was supplemented with controls from two other studies with different research questions but with identical scanning protocols. Consequently, AUD specific clinical measures were not available for the 12 supplemented control participants. Therefore we report basic demographics for all 63 participants but only report clinical measures for the AUD patients and the 13 controls from the study about polysubstance use disorder in Table 1.

The screening section of the Structural Clinical Interview for DSM-5 Axis I disorders was administered to all AUD participants. All AUD individuals had moderate or severe AUD and no other moderate or severe substance use disorder. Exclusion criteria for all participants included a history of neurologic disorder, e.g. epilepsy, traumatic brain injury with loss of consciences $>$ 30 min, cerebrovascular disease, a history of general medical disease such as untreated hypertension, diabetes, hypo/hyperthyroidism, and of psychiatric diseases (e.g. major depression, anxiety, trauma, and PTSD).

All AUD participants were also assessed by a battery of in-person interviews and standardized questionnaires that included the Beck Depression Inventory (BDI, Beck et al., 1961), Barratt Impulsivity Scale (BIS-11, Patton et al., 1995), the State-Trait-Anxiety Inventory (STAI; Spielberger and Vagg, 1984), the Alcohol Use Disorder Identification Test (AUDIT; Reinert and Allen, 2002) as well as standardized questionnaires assessing lifetime substance use (alcohol and other substances including tobacco). AUD patients had a history of consuming at least 80 standard alcoholic drinks (1 standard alcoholic drink contains 13.6 g of ethanol) per months ($>$150 for men) for $>$6 years ($>$8 years in men) before treatment. Controls had consumed $<$60 standard alcoholic drinks in any month over lifetime. The Committees on Human Research at the University of California San Francisco and the VA Medical Center had approved the study. Signed informed consent had been obtained from each participant prior to any research procedures in accordance with the Declaration of Helsinki.

2.2. MRI data

The MRI data were collected at the VA Medical Center San Francisco on a 3T MRI scanner (Siemens Magnetom Skyra Syngo MR D13) using a 20 channel receive head coil. The full study protocol included different types of structural images, as well as rs-fMRI and spectroscopy. This report analyzed the images obtained with a T1 weighted MPRAGE

Table 1
Demographics.

	Controls	Relapsers	Abstainers	Significance
Sample Size [N]	25	23	15	
Age [Years]	43.4 (10.2)	42.1 (9.8)	41.1 (10.3)	$p > 0.49$
Male/Female [N]	18 / 7	15 / 8	8 / 7	$p > 0.48$
Education [Years]	16.2 (2.34)	15.1 (2.1)	15 (2.4)	$p > 0.11$
AUDIT	1.8 (1.2)*	31.0 (6.1)	30.6 (6.7)	$p = 0.83$
Lifetime Number of Drinks/Month	7 (6.2)*	193.9 (122.3)	187.2 (96.1)	$p = 0.85$
Onset Age Heavy Drinking [Years]	na	22.9 (7.8)	23.8 (7.5)	$p = 0.72$
Heavy Drinking [Months]	na	178.2 (86.8)	152.5 (71.3)	$p = 0.28$
Abstinence [Days]	na	19.6 (9.9)	20.8 (8.8)	$p = 0.73$
Smoker/Non-Smoker	2 /11*	9/14	2/13	$p = 0.08$
BIS-11	53 (9.2)*	66.4 (11.1)	67.1 (8.8)	$p = 0.82$
BDI	3 (4.3)*	14.7 (7.67)	12.07 (8.6)	$p = 0.34$
STAI State	23 (3.5)*	36.3 (10.8)	36.8 (10.8)	$p = 0.88$
STAI Trait	32 (9.0)*	49.6 (12.1)	46.0 (12.0)	$p = 0.38$
Median Total Days Drinkingduring Scan Interval	na	6 [1–105]	0	
Median Total Number of Drinks during Scan Interval	na	42 [4–1,246]	0	

Group means with the corresponding standard deviations in parentheses. Statistical tests were calculated only for the two AUD groups, the p values reported in the last column on the far right refer to these comparisons. The asterisks indicate that only the values of the 13 control subjects for which these values were collected were used for the calculation of mean and SD. A standard alcoholic drink is defined as containing 13.6 g of pure alcohol. Range in square brackets; AUDIT = Alcohol Use Disorders Identification Test; BIS-11 = Barret Impulsivity Scale, BDI = Beck's Depression Index and STAI = State-Trait-Anxiety Inventory.

sequence with repetition time (TR) = 2300 ms; echo time (TE) = 2.98 ms; flip angle $90^{0,}$ field of view (FOV) 192 × 256 × 256 mm^3, isotropic voxel size 1 × 1 × 1 mm^3, 256 slices per volume, acquisition duration = 5.28 min.

2.3. Voxel-based morphometric analyses

To examine cross-sectional GM differences between the three groups at the two timepoints and group-specific within-subject change over the three-months interval, we computed a VBM using the default longitudinal processing pipeline of the Computational Anatomic Toolbox (CAT12 version 12.7) (http://www.neuro.uni-jena.de/cat/), which is implemented in the Statistical Parametric Mapping Toolbox (SPM12) (http://www.fil.ion.ucl.ac.uk/spm/) and was run on MATLAB R2017b. CAT12 offers two longitudinal pre-processing pipelines, one optimized for subtle changes in response to short-time neuroplastic effects, the other optimized for larger changes in response to ageing, developmental or neurodegenerative effects over longer time periods. We expected only subtle GM changes, since the degree of sobriety-induced plasticity in AUD is highest within the very first few weeks of abstinence (Gazdzinski et al., 2005; Zou et al., 2018), as the baseline scan in our study had not been acquired until the AUD participants had been sober already for one month. Therefore, we chose the longitudinal CAT12 pipeline optimized for subtle changes within time intervals as short as three months for our study.

At first, all T1 weighted images from both time points of each individual participant were realigned using an inverse-consistent rigid-body registration, followed by an intra-subject bias-field correction. The resulting images were then segmented into GM and white matter (WM), and cerebro-spinal fluid (CSF) probability maps reflecting the concentration of the respective tissue within each individual voxel, the deformation to the standard template was estimated, a mean transformation for both timepoints calculated and applied to all individual images, and the tissue maps normalized to the MNI template. In a final step, the resulting modulated and normalized tissue probability maps were smoothed with a 2 mm FWHM smoothing kernel to enhance the regional specificity, since the core regions of the brain reward system consist of relatively small subcortical structures.

2.3.1. Statistical analyses VBM

Age and total intracranial volume ((TIV) Malone et al., 2015) were modeled as covariates of no interest to control for differences of age and head size. An implicit mask was used to ensure that only GM voxels with intensities of 0.1 and higher were included in the analyses. The fit of the implicit mask with the subjects' smoothed GM map was checked by visual inspection.

To test for group differences in voxel-wise GM probability at each timepoint separately, the SPM full factorial model was used to compute a 1 × 3 ANOVA with TIV and age as covariates without interest. The three group contrasts were defined as t-tests: controls vs relapsers, controls vs abstainers, and abstainers vs relapsers. The SPM flexible factorial model with TIV and age as covariates without interest was used to compute within-subject change of GM probability in each group separately. These change contrasts were defined as paired t-tests to test for changes from baseline to follow-up.

The non-parametric Threshold-Free-Cluster-Enhancement (TFCE; permutation with 10,000 iterations) method in combination with the FWE correction (threshold $p = 0.05$ FWE) to control for multiple comparisons were used to detect voxel clusters indicating significant between-group differences and within-subject changes in GM probability. In contrast to other cluster-based thresholding methods, the TFCE method does not assume stationarity (=constant smoothness) of the data, provides better sensitivity as it is less affected by the smoothing kernel used, and does not require the user to arbitrarily specify an initial cluster-forming threshold (Salimi-Khorshidi et al., 2009; Smith and Nichols, 2009).

2.4. Post-hoc GM network analyses in combination with the profile similarity index (PSI)

In a second step, we used a GTA approach to investigate (a) whether the GM network organization differed between the three groups as a result of the local GM reductions detected by the VBM in the two AUD groups, and (b) the degree to which the two AUD groups' GM network organization had changed from baseline to follow-up as a result of their GM volume alterations. GTA is a mathematical branch that uses two basic elements - nodes and links connecting the nodes - to describe complex network structures like the brain. An advantage of GTA compared to other analysis methods is that by combining it with the PSI approach it is not only possible to compare different network architectures between groups and describe how efficiently the brain as a whole is organized, but also to describe the roles of the different nodes within the whole-brain network and how a change of a node's role influences the roles of all other nodes. We used that feature of GTA to understand better how the GM network architecture of the entire brain differed between the three groups and particularly to disentangle how the GM differences in the four frontocerebellar subcircuits between the two AUD groups and controls (as detected by the initial VBM analyses) as well as their potential for change after treatment related to successful abstinence and future relapse.

The nodes for the GTA were defined with the AICHA parcellation (Joliot et al., 2015) complemented by the 32 cerebellar regions of interest (ROI) of the AAL atlas (Tzourio-Mazoyer et al., 2002), since the

AICHA partition does not include the cerebellum. The PSI metric (Mueller et al., 2014) was used to define the edges between the 416 nodes. The steps necessary for computing GM PSI connectivity matrices from individual normalized modulated GM tissue maps were described in detail in Mueller and Meyerhoff (2021) and are illustrated in Fig. 1. In short, the following steps were involved: The individual, smoothed, normalized, and modulated GM probability maps (Fig. 1, step **A**) were corrected for TIV and age differences and then transformed into z-scored GM maps (Fig. 1, step **B**). The AICHA parcellation supplemented by the cerebellar nodes was then used to partition the TIV- and age-corrected z-score maps into 416 ROIs and the mean z-score of each ROI was extracted (Fig. 1, step **C**). The global mean of the z-scored GM maps of all 25 controls at baseline was computed and used as reference for computing of the individual timepoint-specific PSI connectivity matrices of all participants (Fig. 1, step **D**). A PSI matrix always has both positive and negative entries. However, since we are particularly interested here in describing how the GM network of the two AUD groups differs from the controls due to the local GM reduction, only the meaning of a negative entry is of interest. A negative entry in the PSI matrix indicates that both brain regions have lower z-scored GM values than the global z-scored GM value of the controls at baseline and that therefore both brain regions are atrophic relative to controls at baseline. Additionally, independent from the sign of a PSI entry, the PSI value is higher (lower) the more similar (dissimilar) the two brain regions' z-scored GM values are.

The resulting PSI matrices were then used to compute the GTA measure of weighted negative strength for each of the 416 nodes in the PSI matrix (Fig. 1, step **E**) using the respective GTA metric from the BCT toolbox (Rubinov and Sporns, 2010). The negative strength of a node equals the weighted sum of all negative PSI connections of the node in question. In that context, a high negative strength value means that many other nodes share the same degree of atrophy relative to the reference group with the node in question and is an indicator for diffuse atrophy.

To get a better understanding of how the GM network architecture of the entire brain differs between the controls and the two AUD groups, we computed the negative nodal strength of all 416 individual nodes for each participant at each timepoint. For easier interpretability, we then built 10 AICHA composites representing the gross anatomy of the brain (frontal lobe, temporal lobe, parietal lobe, occipital lobe, cerebellum, insular cortex, sensorimotor cortex, limbic cortex and the subcortical structures thalamus and basal ganglia) and calculated their average negative strength. Additionally, we computed the global negative strength value by averaging the negative strength values of 416 nodes as a simple proxy for the two AUD groups' degree of diffuse global atrophy relative to controls.

Next, we wanted to better understand the degree to which the observed GM reductions and any GM recovery from baseline to follow-up related specifically to the frontocerebellar circuit. To that aim, we took advantage of the fact that this circuit can be further differentiated into four functionally separate subcircuits known as the DMN subcircuit, ECN subcircuit, SAL subcircuit, and SMN subcircuit (Krienen and Buckner, 2009; Habas et al., 2009; Buckner et al., 2011). The selection of the ROIs/nodes to create AICHA composites of these four frontocerebellar subcircuits was guided by previous descriptions (Krienen and Buckner, 2009; Habas et al., 2009; Buckner et al., 2011), including a more precise identification of the thalamic and striatal subregions projecting to the frontal cortex (Zhang et al., 2008), and of the subcortical regions of the DMN (Alves et al., 2019). After having thusly identified the AICHA nodes that corresponded most closely to the four subcircuits (Fig. 2), we computed for each subcircuit a new participant- and timepoint-specific PSI connectivity matrix built only from the nodes of the respective subcircuits. Next, these new PSI matrices were used as input to calculate a single global negative strength value for each subcircuit by averaging the negative strength values across all individual nodes of the respective subcircuit (Fig. 1, step **F**). The result was a single participant- and timepoint-specific negative strength value for each subcircuit restricted to the connections between the nodes belonging to the same subcircuit (=internal negative strength, Fig. 1, step **G**). A subcircuit's mean internal negative strength quantifies how similar the degree of atrophy is between the brain regions belonging to the same subcircuit in relation to the average GM probability value in the reference group, i.e. controls at baseline. Therefore, a high internal negative strength value means that all constituent regions of the subcircuit are similarly atrophic, whereas a small internal negative strength value indicates a heterogeneous degree of atrophy among the constituent regions of the subcircuit, with some regions being "atrophy hotspots".

In a final step, we calculated the mean external negative strength of

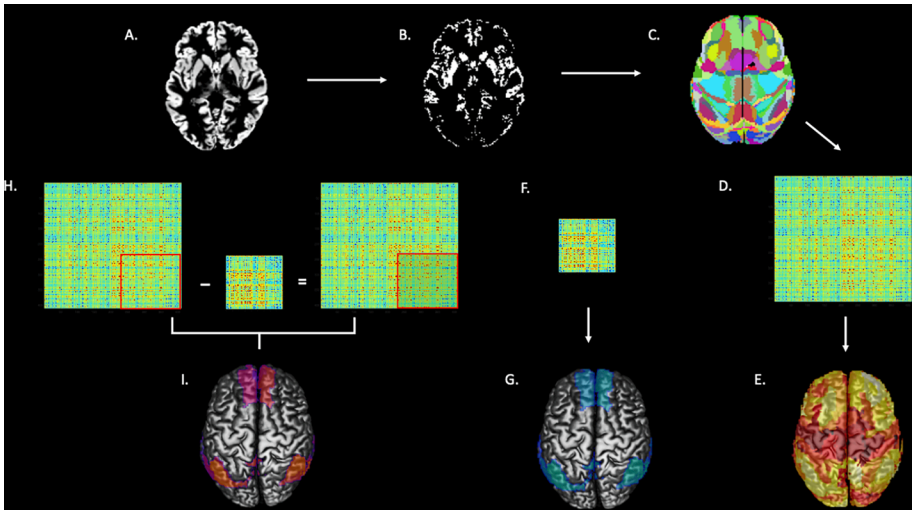

Fig. 1. Graphical description of the computing of a profile similarity index (PSI) matrix, internal and external negative nodal strength for one of subcircuits. The input to compute a PSI matrix is an individual, normalized gray matter map (A). The gray matter map is corrected for age and total intercranial volume and then z-scored, resulting in (B). Next, the AICHA parcellation (C) is used to extract the mean gray matter intensity of each of the 416 regions of interest or nodes from (B) and used to compute a PSI connectivity matrix (D). In this matrix, a negative entry for two nodes codes the information that both nodes have a mean GM amount that is lower than the global mean GM amount of the reference group (=controls at baseline), and a positive entry codes the information that at least one of the nodes has a mean gray matter amount higher than the global mean GM amount of the reference group. In a next step, the negative strength of all nodes is computed using the PSI connectivity matrix as input, resulting in (E). (E) illustrates the negative strength distribution across the entire brain, darker orange color codes nodes with lower negative strength values, lighter orange – yellow color codes nodes with higher negative strength values. Next, the steps C – E are repeated but only the nodes forming the default mode network (DMN) subcircuit are used to compute the PSI connectivity matrix resulting in (F). Again, negative strength is computed from E, resulting in G, which shows the internal negative strength distribution of the DMN subcircuit. In a last step, the DMN-nodes-only PSI connectivity matrix (F) is subtracted from the corresponding nodes (location in matrix is highlighted by the red rectangle) of the entire-brain PSI matrix (D) and negative strength is anew computed form the nodes within the shaded rectangle resulting in external strength of the DMN subcircuit (I).

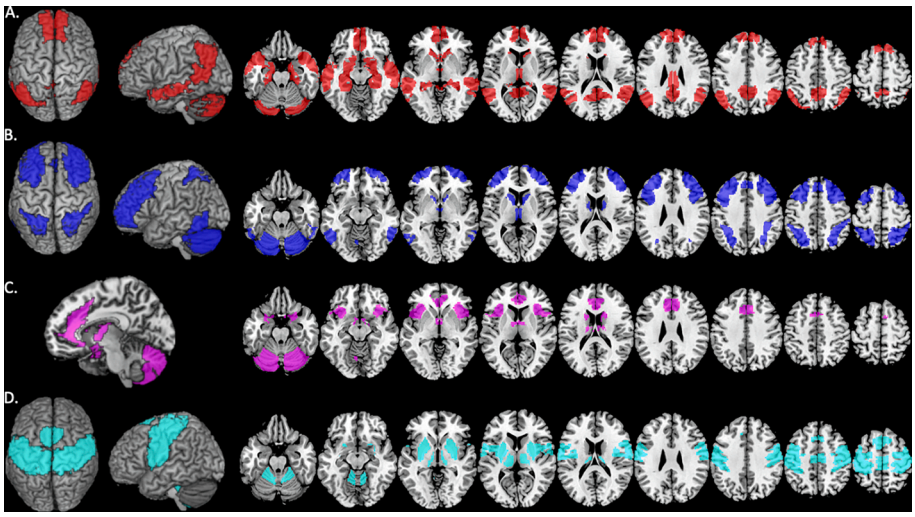

Fig. 2. The four frontocerebellar subcircuits. Anatomical location of the four fronto-cerebellar subcircuits. Default mode network subcircuit (A), executive-control network subcircuit (B), salience network subcircuit (C), sensorimotor network subcircuit (D).

each subcircuit with the rest of the brain. For this purpose, we first subtracted the individual internal negative strength value of each node in a specific subcircuit from its individual negative strength value that we had computed using the PSI Matrix with all 416 nodes (Fig. 1, step **E**) and then averaged these subtraction results across all nodes belonging to the same subcircuit to yield a single value that quantified the external negative connectivity of the subcircuit to the rest of the brain (=external negative strength, Fig. 1, steps **H** and **I**). A subcircuit's mean external negative strength relates its atrophy to the degree of global atrophy of the rest of the brain. A high (low) external negative strength value indicates that the subcircuit's degree of atrophy is in the same range (greater) than the atrophy of the brain regions outside the subcircuit.

2.4.1. Statistical analysis GTA

Since the negative strength values were not normally distributed, we used non-parametric Wilcoxon Rank Sum tests for group comparisons and Wilcoxon Signed Rank tests to assess within-group change from baseline to follow-up. The Bonferroni method with a critical value q = 0.05 was used to correct for multiple comparisons as indicated in the Table legends.

3. Results

3.1. Demographics

The three participant groups did not differ significantly from each other in age, sex, or years of education (see Table 1). In addition, the relapser and abstainer groups did not significantly differ from each other on proportion of smokers, in BIS-11, BDI, STAI or AUDIT, lifetime alcohol intake per month, or duration of abstinence at baseline.

3.2. Global atrophy and global tissue volumes: Cross-sectional and longitudinal findings

At baseline, both abstainers and relapsers showed significantly higher TIV/brain size than controls indicating global atrophy, but the two AUD groups did not significantly differ on this measure (see Table 2). At follow-up, however, TIV/brain size was significantly higher in relapsers compared to either abstainers or controls. Relapsers at both timepoints had significantly smaller absolute GM, WM, and larger CSF volumes than controls (Table 2**)**. Abstainers, on the other hand, significantly differed from controls in GM and CSF only at baseline, due to a significant increase in GM volume during the three-months interval.

Table 2
Group comparisons of total intracranial volume, brain atrophy, global gray and white matter volume.

	Controls	Relapsers	Abstainers
TIV			
Baseline	1495.8 (123.32)	1499.94 (94.01)	1529.08 (146.43)
Follow-Up	1495.45 (122.11)	1497.08 (87.83)	1522.42 (147.08)
Global Atrophy			
Baseline	1.25 (0.048)	1.32 (0.065) °°	1.29 (0.060) *
Follow-Up	1.25 (0.049)	1.31 (0.071) °°	1.26 (0.054) ⊗
Global GM [cm^3]			
Baseline	655.97 (56.01)	622.80 (47.11) °°	644.97 (50.09) *
Follow-Up	653.06 (50.95)	625.20 (50.11) °	657.34 (54.30) ‡‡
Global WM [cm^3]			
Baseline	540.31 (45.3)	516.20 (50.05) °°	536.56 (51.04)
Follow-Up	541.25 (47.13)	517.63 (55.24) °	548.09 (53.35) ⊗ ‡‡
Global CSF [cm^3]			
Baseline	298.73 (58.07)	359.55 (59.21) °°	345.64 (79.35) *
Follow-Up	300.16 (59.78)	352.86 (60.34) °°	315.14 (71.87) ⊗ ‡‡

Global atrophy (= TIV/(Global GM + Global WM) and mean global tissue volumes for gray matter (GM), white matter (WM), and cerebrospinal fluid (CSF) before total intercranial volume (TIV) and age correction, standard deviations in parentheses. Significant differences between the three groups are coded as follows: ° after TIV correction significant difference between controls and relapsers at $p < 0.05$; °° after TIV correction significant difference between controls and relapsers at $p < 0.005$; * after TIV correction significant difference between controls and abstainers at $p < 0.05$; ⊗ after TIV correction significant difference between relapsers and abstainers at $p < 0.05$; ‡‡ after TIV correction significant change in abstainers at $p < 0.005$.

Abstainers also showed a significant increase in global WM volume to the effect that they had significantly more global WM volume than relapsers at follow-up. The corresponding CSF volume changes were also observed.

3.3. Voxel based morphometry (VBM): Cross-sectional and longitudinal findings

At baseline, relapsers presented with significantly less GM in 12 clusters encompassing 51,834 voxels (Fig. 3**A** in the main text and Table S1 with the detailed VBM results in the supplement). The largest cluster had its peak in the right thalamus and covered over 49,516 voxels or 95.5% of all voxels showing GM reduction. The cluster

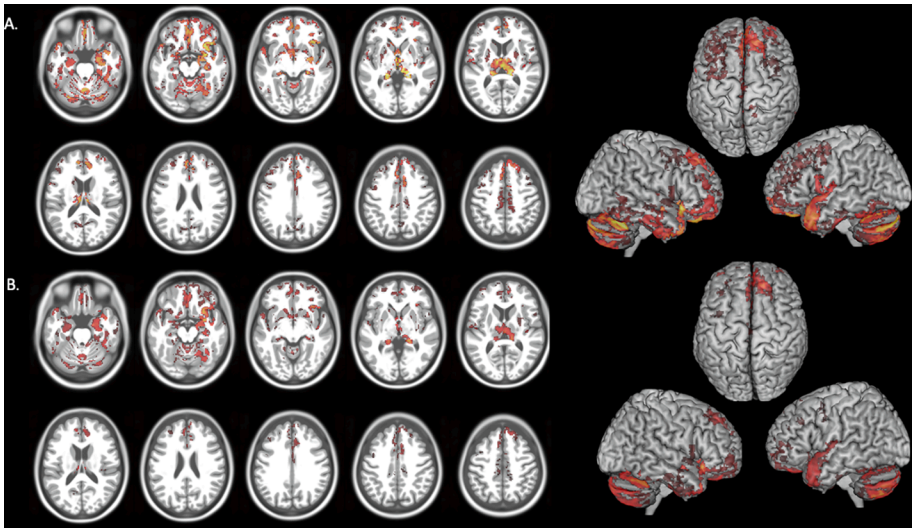

Fig. 3. Gray matter reduction in relapsers relative to controls at baseline and follow-up. Brain regions showing significant gray matter (GM) reduction in relapsers relative to controls at baseline (A). Brain regions showing significant GM reduction in relapsers relative to controls at follow-up (B). Red colored brain regions = significant GM reduction at $p < 0.05$ FWE corr., yellow colored brain regions = significant GM reduction at $p < 0.001$ FWE corr.

extended from there into the left thalamus and bilaterally into the amygdala, putamen and caudate nucleus, hippocampus and adjoining parahippocampal gyri. Cortically, this large cluster bilaterally covered parts of the anterior cingulum gyrus, gyrus rectus, middle and lateral orbital gyri, anterior insula, middle frontal, and superior frontal, precentral, and superior temporal gyri, temporal pole, precuneus and anterior and posterior cerebellum. The other 11 clusters were observed in the cerebellum, frontal and adjoining precentral, bilateral temporal and visual cortices.

In contrast, abstainers at baseline showed GM reduction relative to controls in 8 clusters covering only 4,809 voxels, which is about 11% of the GM reduction found in relapsers at that timepoint (Fig. 4**A,** Table S2). However, just as in the relapsers, the abstainers' most prominent cluster had its peak in the right thalamus and extended into the left thalamus; it included 1,772 voxels constituting 36.8 % of all voxels with GM reduction at baseline. The other 7 clusters were located in the right pars orbitalis and fusiform gyrus, right and left amygdala, as well as left pars opercularis and thalamus. However, although the relapsers' thalamus cluster was almost 28 time larger than the abstainers' cluster, we did not observe any statistically significant regional differences in GM volumes between the two AUD groups at baseline.

Three months later at follow-up, and although they had resumed consuming alcohol, relapsers showed smaller regions of GM loss relative to controls than at baseline, with 16 clusters encompassing 35,145 voxels (Fig. 3**B**, Table S3). The most extended cluster with 32,642 voxels or 92.9% of all voxels showing significant GM reduction covered the same subcortical and cortical regions as at baseline, except for the left middle frontal gyrus and the bilateral temporal and lateral occipital regions – tissue volumes in those regions seemed to have increased relative to controls. The other clusters of reduced GM were located in the right frontal cortex, cingulate gyrus, inferior and superior temporal gyri, precuneus and caudate nucleus. In contrast, regional GM volumes in abstainers at follow-up did no longer differ significantly in GM from those in controls. Nevertheless, despite this apparent GM volume recovery in abstainers, the two AUD groups did not differ significantly in any regional GM volume at follow-up.

Although GM increased in both AUD groups from baseline to follow-up (as expressed by the number of voxels with significantly less GM

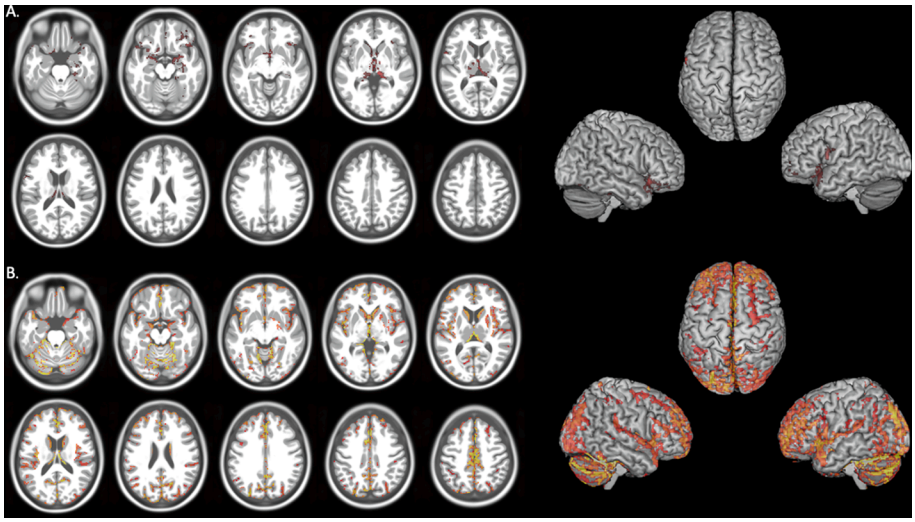

Fig. 4. Gray matter reduction in abstainers relative to controls at baseline and gray matter increase in abstainers from baseline to follow-up. Red color indicates brain regions with significant reduction in gray matter (GM) in abstainers relative to controls at $p < 0.05$ FWE corr. (A). Red color indicates brain regions with significant increase of GM at $p < 0.05$ FWE corr., yellow color indicates significant GM increase at $p < 0.001$ FWE corr. (B).

relative to the controls at the respective time point), only the abstainers' GM increase was significant, occurring in 13 clusters (40,763 voxels) throughout the brain (Fig. 4**B,** Table S4). Fig. 5 shows that especially brain regions without significant GM reduction at baseline had undergone significant volume increases by follow-up. The most extensive cluster (37,764 voxels) of GM increase in the abstainers had its peak voxel in the right cerebellum (lobule VI) and extended from the cerebellum into the caudal to the rostral midline of the brain, further covering bilateral lateral and medial frontal regions, bilateral insula, the posterior bilateral parts of the thalamus, the head of the caudate nucleus, and right putamen. The other clusters of volume increases were mainly located in the left hemisphere (postcentral, angular, inferior parietal, and middle temporal gyri), except for the right middle occipital gyrus and right hippocampus.

3.4. Post-hoc GM network analyses: cross-sectional and longitudinal negative strength findings

3.4.1. Global and gross anatomical negative strength

The global negative strength over all 416 ROIs is a proxy for diffuse global atrophy. Relapsers and abstainers at both timepoints had significantly higher global negative strength values than the controls, indicating a persistent and diffuse global atrophy of the entire brain in both AUD groups relative to controls (Table 3). Abstainers and relapsers, however, did not differ significantly on this global measure at either timepoint (baseline: $p = 0.36$; $r = 0.06$; follow-up: $p = 0.57$; $r = 0.09$), although a numerical decrease in this proxy measure at follow-up indicated some global volume recovery in both AUD groups.

Fig. 6 shows that the negative strength distribution pattern across the entire brain was preserved in the two AUD groups, although with globally higher negative strength values than in controls. Consequently, all groups had similar distributions, with the frontal, temporal, parietal, occipital cortices and cerebellum showing the highest negative strength values (orange in controls vs yellow in the AUD groups) and insula and sensorimotor cortex, the limbic system, thalamus and basal ganglia showing the lowest negative strength values (dark red in controls vs red in the AUD groups).

Wilcoxon Rank Sum tests revealed the timepoint-specific group differences in negative strength at the level of the gross anatomical AICHA composites, further clarifying the distribution pattern (Table 3). At both timepoints, both AUD groups had significantly higher negative strength values than controls in the frontal, sensorimotor, temporal and parietal composites. Additionally, only relapsers had significantly higher negative strength values than controls in the cerebellum and limbic system at both timepoints, and in the occipital cortex and thalamus at baseline only. In addition, abstainers at baseline had significantly higher negative strength values than controls in insular and occipital cortices, the limbic system, and the thalamus, reflecting atrophy that was no longer observed at follow-up after continued abstinence.

Quantitatively, the thalamus, insula, temporal lobe, and the limbic system in both AUD groups at both timepoints, the cerebellum in relapsers at both timepoints, and the cerebellum in abstainers at baseline belonged to the five brain regions with the highest negative strength differences relative to controls (Table 3). Longitudinally over the three-months interval, thalamus (−1.99 in relapsers and −1.74 in abstainers) and cerebellum (−1.41 in relapsers and −1.31 in abstainers) were the regions with the greatest recovery in negative strength (Table 3).

3.4.2. Internal negative strength of the four subcircuits

At baseline, relapsers had significantly higher internal negative strength values in all four subcircuits than controls. By contrast, abstainers at baseline had significantly higher internal negative strength values than controls in the subcircuits of the DMN and ECN only (Table 4 and Fig. S1 in the supplement). Three months later, relapsers had still significantly higher internal negative strength in DMN-, ECN-, and SMN-subcircuits than controls, whereas the SAL-subcircuit value was similar to that of the controls. In contrast, none of the abstainers' subcircuits at follow-up showed a significant difference in internal negative strength compared to the controls. The internal negative strength values of the abstainers' and relapsers' subcircuits did not differ significantly at any point in time (Table 6). Although both AUD groups showed a reduction in internal negative strength values from baseline to follow-up, only the decrease in the DMN subcircuit of the abstainers survived a Bonferroni correction for four simultaneous comparisons.

3.4.3. External negative strength of the four subcircuits

At both timepoints, relapsers and abstainers had across all four subcircuits significantly higher external negative strength values than controls (Table 5 and Fig. S2 in the supplement), with no significant differences between the two AUD groups at either timepoint. The mean external negative strength values of all four subcircuits decreased from baseline to follow-up in both abstainers and relapsers, and the large decrease in the relapsers' SAL-subcircuit value was statistically significant ($p = 0.012$) (Table 6). However, this change did not survive a subsequent Bonferroni correction for four simultaneous comparisons.

4. Discussion

The aims of this study in treatment-seekers with AUD were a) to investigate the degree to which GM reduction specifically in the frontocerebellar circuit early in treatment relates to subsequent abstinence and relapse, and b) to measure the degree to which AUD-related GM reduction in the frontocerebellar circuit alters the GM network architecture of the entire brain and influences the integration of four prominent frontocerebellar subcircuits within the brain's GM network architecture.

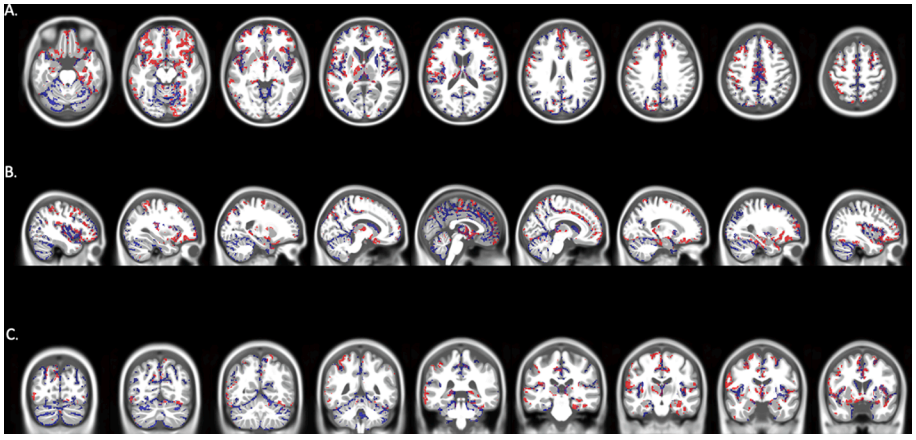

Fig. 5. Regions of AUD-related gray matter reductions in abstainers do not correspond to the regions of gray matter recovery in abstainers. Axial plane (A), sagittal plane (B), and coronal plane (C) indicate the brain regions with GM reduction in abstainers at baseline relative to controls (red color) and the GM increase pattern in abstainers at follow-up (blue color). The blue recovery pattern is shown at 0.05 FWE corrected, the red reduction pattern at 0.001 uncorrected to allow for an easier comparison of the two patterns. The overlap of the two pattern is minimal, mainly in the lateral and medial part of the motor cortex. Otherwise, the two patterns cover different brain regions.

Table 3
Group differences and change in negative strength on global and gross anatomical level.

Negative Strength Baseline	Controls	Relapsers	Abstainers
Frontal	7.59 (5.72)	14.11 (4.49; 0.65)*	12.66 (5.14; −0.59)*
Insula	3.45 (4.57)	7.35 (6.83; 0.44)	8.81 (5.35; −0.57)*
Sensorimotor	4.48 (1.96)	7.58 (2.62; 0.56)*	7.75 (4.18; −0.61)*
Temporal	4.93 (3.29)	9.73 (5.08; 0.58)*	8.61 (4.31; −0.59)*
Parietal	6.79 (3.24)	12.00 (4.33; 0.59)*	11.30 (3.75; −0.61)*
Occipital	7.91 (5.17)	11.00 (5.54; 0.48)*	11.22 (4.36; −0.52)*
Limbic	3.50 (2.56)	7.65 (3.32; 0.56)*	7.25 (3.99; −0.58)*
Thalamus	3.58 (3.82)	8.98 (7.65; 0.61)*	9.41 (6.71; −0.54)*
Basal Ganglia	3.57 (3.39)	6.34 (4.99; 0.39)	5.23 (4.36; −0.-29)
Cerebellum	5.16 (3.20)	11.31 (7.62; 0.60)*	9.48 (4.92; −0.48)
Global	5.82 (3.57)	10.29 (3.47; 0.64)*	9.45 (3.45; −0.64)*
Negative Strength Follow-Up	**Controls**	**Relapsers**	**Abstainers**
Frontal	7.45 (5.92)	13.54 (5.35; 0.59)*	12.59 (4.40; −0.56)*
Insula	3.60 (4.81)	8.08 (5.25; 0.41)	7.92 (4.11; −0.48)
Sensorimotor	4.41 (2.75)	7.35 (4.25; 0.53)*	7.57 (1.99; −0.64)*
Temporal	5.36 (3.28)	9.73 (3.98; 0.54)*	8.45 (1.86; −0.53)*
Parietal	7.36 (3.64)	11.90 (3.48; 0.56)*	10.48 (2.65; −0.56)*
Occipital	8.44 (5.56)	10.68 (5.68; 0.43)	10.87 (2.90; −0.44)
Limbic	4.06 (2.33)	7.47 (3.67; 0.51)*	6.35 (2.80; −0.48)
Thalamus	4.60 (4.97)	7.33 (6.94; 0.44)	7.67 (3.48; −0.46)
Basal Ganglia	4.09 (3.71)	6.23 (4.21; 0.32)	4.93 (6.60; −0.11)
Cerebellum	4.74 (4.27)	9.66 (6.75; 0.52)*	8.16 (4.55; −0.41)
Global	6.10 (3.63)	9.53 (4.20; 0.58)*	9.25 (1.39; −0.58)*
Change Negative Strength	**Controls**	**Relapsers**	**Abstainers**
Frontal	−0.14	−0.72	−0.06
Insula	0.15	0.58	−0.89
Sensorimotor	−0.07	−0.34	−0.18
Temporal	0.43	−0.13	−0.16
Parietal	0.57	−0.16	−0.82
Occipital	0.52	−0.34	−0.36
Limbic	0.56	−0.2	−0.89
Thalamus	1.01	−1.99	−1.74
Basal Ganglia	0.52	0.35	−0.31
Cerebellum	−0.42	−1.41	−1.31
Global	0.27	−0.77	−0.19

Values are median with interquartile distance and effect size r in parentheses, asterisk = significant difference at $p < 0.05$ relative to controls at the same timepoint (Bonferroni corrected for 33 simultaneous comparisons); change was computed by subtracting the median value at baseline from median at follow-up.

The VBM analysis revealed that relapsers (who were sober at baseline but had relapsed before follow-up three months later) showed significant whole-brain GM reductions relative to controls at both timepoints but no significant GM change over the three-months interval from baseline to follow-up; on the other hand, abstainers showed significant GM reduction relative to controls only at baseline and had experienced significant GM recovery at follow-up. Chronic alcohol-associated cortical atrophy is a common finding in the alcohol neuroimaging literature (Xiao et al., 2015; Yang et al., 2016). The recovery found in abstainers of this study after four months of sobriety also agrees with previous longitudinal research (reviewed in Meyerhoff and Durazzo, 2020). Despite these GM volume increases in abstainers over time, abstainers did not differ significantly from relapsers on their cross-sectional or longitudinal VBM metrics. On the other hand, the newly applied GTA approach proved to be more sensitive to brain morphometry in treatment seeking AUD individuals than the more conventional VBM analyses. It was not only able to detect a lasting and specific, AUD-related imprint on the whole-brain GM network architecture in both AUD groups at follow-up, but it also revealed subcircuit-specific differences in recovery between abstainers and relapsers. In the following sections, we discuss our findings in more detail.

4.1. Local group differences and within-group changes in GM

The VBM revealed that both AUD groups at baseline had several extensive clusters with significant GM reduction compared to controls. In both AUD groups, the thalamus was in the center of the most extensive cluster, but this cluster was 28 times larger in future relapsers than future abstainers. The degree of GM damage to the thalamus (GM reduction compared to controls in 1,372 voxels or 46.6% of all thalamus voxels in relapsers vs 492 voxels or 16.7% of all thalamus voxels in abstainers) early into treatment is related to treatment success in AUD. This finding is consistent with an earlier report (Segobin et al., 2014) in which the thalamus' GM volume loss before treatment was related to future relapse. That the degree of structural damage to the thalamus may be a key factor for treatment outcome in AUD must be placed in the context of the thalamus' role for integrating multidimensional information across the brain (Müller et al., 2020). This brain structure not only relays first-order sensory information to the cortex (Habas et al., 2019; Halassa and Sherman, 2019; Sherman, 2007, 2016, 2017; Usrey and Sherman, 2019), but it is also involved in a wide variety of higher-order cognitive functions (Habas et al., 2019; Pergola et al., 2018), with its subunits capable of dynamically integrating multimodal information from diverse networks (Garrett et al., 2018; Hwang et al., 2017). The importance of the functional integrity of the thalamus for successful alcohol abstinence was recently also demonstrated in a resting-state fMRI study by our team with an AUD patient group similar to that described here: One month into treatment, future relapsers differed from healthy controls and future abstainers in the way the thalamus interacted with major resting-state networks (Muller and Meyerhoff, 2021).

Except for the thalamus, the only other brain regions of GM loss in both AUD groups compared to controls were the bilateral insula and the medial parts of the orbitofrontal cortex. Neither is specific for AUD, but they belong to those brain regions that are generally atrophied in substance use disorder, independent of the addictive substance (Mackey et al., 2019; Navarri et al., 2020). In addition to the three brain regions that they had in common with abstainers, the relapsers' "thalamus" cluster at baseline and follow-up covered large parts of the bilateral medial and lateral superior frontal cortex and the cerebellum, all main constituent regions of the frontocerebellar circuit that is uniquely targeted by AUD (Cardenas et al., 2007; Pitel et al., 2015; Segobin, et al., 2019; Sullivan et al., 2003; Mackey et al., 2019). Although the two AUD groups did not significantly differ in any of the assessed AUD-related behavioral characteristics, the more widespread GM reduction in the frontocerebellar circuit of relapsers compared to abstainers suggests a higher vulnerability in relapsers to the effects of AUD. The structural integrity of the frontocerebellar circuit and specifically the thalamus very early in treatment may therefore be a potential biomarker for future relapse risk.

Interestingly, abstainers showed significant GM recovery in the frontocerebellar circuit at follow-up, although, with exception of the

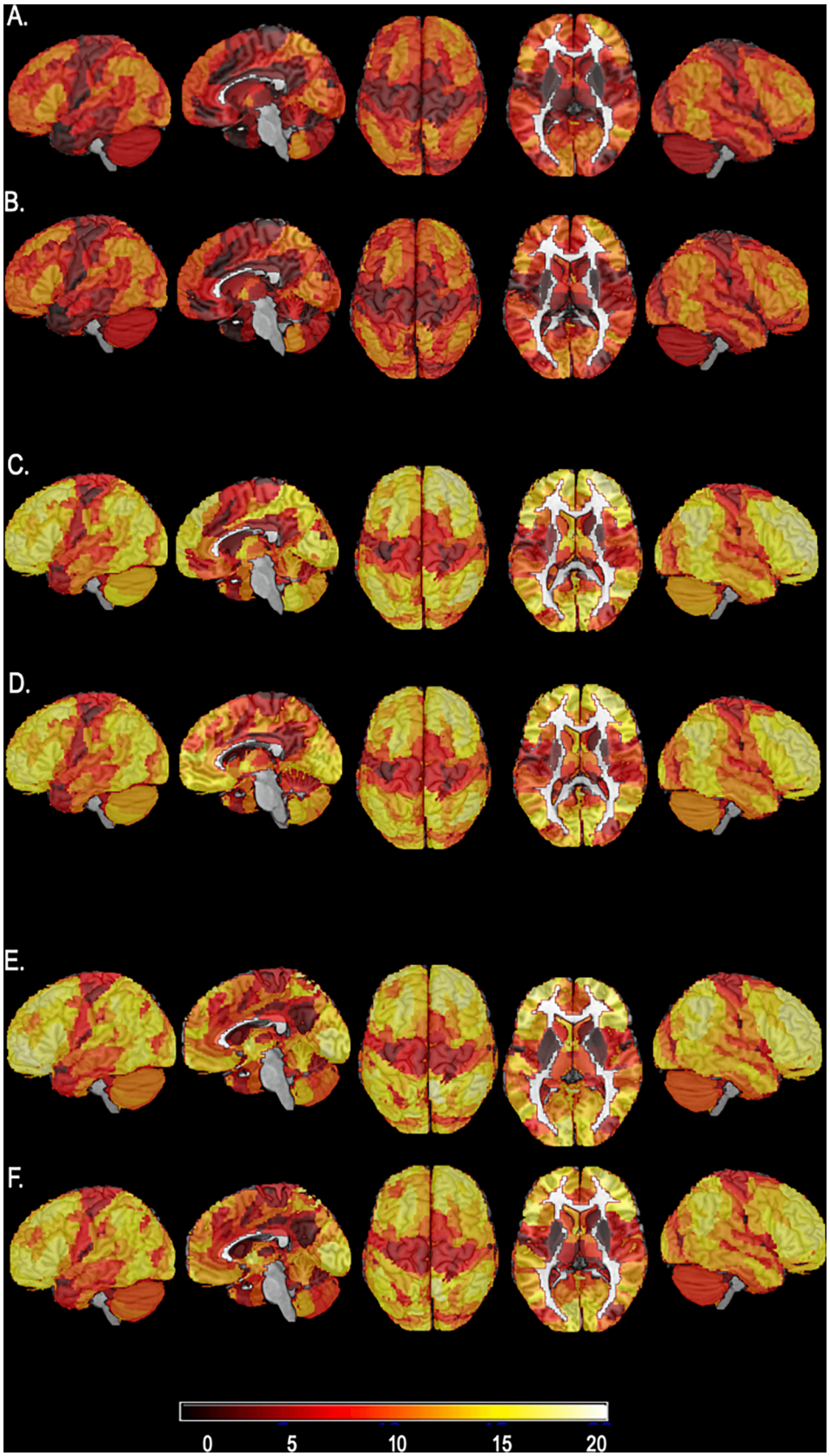

Fig. 6. Negative strength network organization of the entire brain. Negative strength distribution on nodal level for the controls at baseline (A) and follow-up (B), for relapsers at baseline (C) and follow-up (D), and for abstainers at baseline (E) and follow-up (F). A dark brown color indicates a negative strength value of 0 and a light-yellow color a negative strength value of 20. Controls at both timepoints have visibly darker orange hues (corresponding to a negative strength range from 0.1 to 13.5 and a mean = 6.3) than the two AUD groups with relapsers having negative strength values in the range from 0.7 to 18.5 mean = 10.1, and abstainers having negative strength values in the range from 0.4 to 18.5, mean = 9.8. The global negative strength organization is largely preserved in the two patient groups. Brain regions that have a darker hue in controls have also a relative darker hue in the two patient groups, e.g., motor cortex and temporal pole. This indicates that the two patient groups are rather characterized by a global and diffuse atrophy pattern relative to controls than by focal atrophy in specific brain regions.

Table 4
Group differences in internal negative strength in the four frontocerebellar subcircuits.

	Baseline			
	DMN	ECN	SAL	SMN
Controls	1.31/1.34/0.43	1.95/1.84/0.93	0.36/0.29/0.34	0.51/0.49/0.28
Relapsers	2.28/2.31/0.73	3.12/3.24/0.71	0.75/0.78/0.39	0.94/0.85/0.54
Abstainers	2.43/2.13/1.48	3.06/3.22/1.18	0.56/0.60/063	1.01/0.89/1.04
Group Statistics				
Relapsers vs Controls	**p < 0.0001 (0.59)**	**p < 0.0001 (0.70)**	**p = 0.0001 (0.55)**	**p < 0.0001 (0.59)**
Abstainers vs Controls	**p < 0.0001 (−0.65)**	**p = 0.0002 (−0.59)**	p = 0.057 (−0.30)	*p = 0.0021 (−0.49)*
Abstainers vs Relapsers	p = 0.90 (−0.02)	p = 0.83 (0.03)	p = 0.11 (0.26)	p = 0.95 (−0.01)
	Follow-Up			
	DMN	**ECN**	**SAL**	**SMN**
Controls	1.36/1.22/0.72	2.02/2.07/1.09	0.39/0.36/0.39	0.53/0.48/0.34
Relapsers	2.15/2.03/0.71	3.10/2.90/1.35	0.67/0.59/0.65	1.01/1.04/0.85
Abstainers	1.99/1.69/0.91	2.72/2.98/1.54	0.48/0.42/0.31	0.95/0.89/0.66
Group Statistics				
Relapsers vs Controls	**p < 0.0001 (0.56)**	**p < 0.0001 (0.60)**	*p = 0.0047 (0.41)*	**p = 0.0008 (0.48)**
Abstainers vs Controls	*p = 0.0034 (−0.46)*	*p = 0.0119 (−0.40)*	p = 0.59 (−0.08)	*p = 0.0021 (−0.49)*
Abstainers vs Relapsers	p = 0.24 (0.19)	p = 0.67 (0.07)	p = 0.06 (0.30)	p = 0.79 (0.04)

Mean, median and interquartile distance for the four frontocerebellar subcircuits' internal negative strength for each group at baseline (top half) and follow-up (bottom half), together with the group statistics (by Wilcoxon Rank Sum tests). DMN = default mode network subcircuit, ECN = executive-control network subcircuit, SAL = salience network subcircuit, SMN = sensorimotor network subcircuit. Significant p-values are highlighted in italic letters, p-values that survived a Bonferroni correction for 24 simultaneous comparisons are highlighted in bold letters. Effect sizes r (after Rosenthal, 1994) are given in parentheses.

Table 5
Group differences in external negative strength in the four frontocerebellar subcircuits.

	Baseline			
	DMN	**ECN**	**SAL**	**SMN**
Controls	4.15/3.84/2.37	5.91/5.43/3.24	4.79/4.27/3.32	3.94/3.74/1.68
Relapsers	7.04/7.14/2.94	9.91/10.07/3.36	9.03/8.64/4.31	6.53/6.58/2.62
Abstainers	6.89/6.53/1.84	9.47/9.36/4.26	8.34/6.81/4.66	6.78/6.35/3.26
Group Statistics				
Relapsers vs Controls	**p < 0.0001 (0.61)**	**p < 0.0001 (0.65)**	**p < 0.0001 (0.66)**	**p < 0.0001 (0.61)**
Abstainers vs Controls	**p < 0.0001 (−0.60)**	**p < 0.0001 (−0.64)**	**p = 0.0007 (−0.53)**	**p = 0.0001 (−0.61)**
Abstainers vs Relapsers	p = 0.47 (0.12)	p = 0.47 (0.12)	p = 0.34 (0.15)	p = 0.98 (0.01)
	Follow-Up			
	DMN	**ECN**	**SAL**	**SMN**
Controls	4.30/4.12/2.36	6.03/5.45/3.27	5.06/4.92/2.89	4.13/3.76/2.20
Relapsers	6.81/6.60/3.65	9.45/9.05/3.17	8.53/8.60/4.27	6.25/5.91/3.28
Abstainers	6.58/6.40/1.31	9.01/8.94/2.31	7.73/7.56/1.90	6.36/6.05/2.08
Group Statistics				
Relapsers vs Controls	**p < 0.0001 (0.59)**	**p < 0.0001 (0.62)**	**p < 0.0001 (0.59)**	**p = 0.0002 (0.53)**
Abstainers vs Controls	**p = 0.0004 (−0.56)**	**p = 0.0003 (−0.57)**	**p = 0.0014 (−0.50)**	**p = 0.0002 (−0.59)**
Abstainers vs Relapsers	p = 0.49 (0.11)	p = 0.42 (0.13)	p = 0.27 (0.18)	p = 0.74 (−0.05)

Mean, median and interquartile distance for the four frontocerebellar subcircuits' internal negative strength for each group at baseline (top half) and follow-up (bottom half), together with the group statistics (by Wilcoxon Rank Sum tests). DMN = default mode network subcircuit, ECN = executive-control network subcircuit, SAL = salience network subcircuit, SMN = sensorimotor network subcircuit. Significant p-values are highlighted in italic letters, p-values that survived a Bonferroni correction for 24 simultaneous comparisons are highlighted in bold letters. Effect sizes r (after Rosenthal, 1994) are given in parentheses.

thalamus, this circuit had not shown significant GM reduction relative to controls at baseline. Additionally, abstainers at follow-up did no longer exhibit significant GM reduction in the brain regions atrophied at baseline, indicating that these regions must also have recovered to some degree during the three-months interval but not as much as regions with preserved GM at baseline. These three observations combined suggest, on the one hand, that recovery in AUD involves distinct neural processes rather than just being a reversal of any AUD-related GM damage (see Fig. 4), and on the other hand, that abstainers did not simply undergo a regionally localized GM recovery (as suggested by the clearly defined VBM change pattern), but that they also must have experienced a global and rather diffuse GM recovery. The latter was not directly captured by the VBM but could only be indirectly inferred by combining the cross-sectional findings for abstainers at both timepoints relative to controls with the abstainers' recovery pattern at follow-up.

Another aspect regarding the GM recovery in abstainers deserves attention: Although only abstainers recovered GM to such a degree that they did not differ significantly from controls at follow-up, we were unable to observe a significant GM difference between relapsers and abstainers at that time point. As GM volume in relapsers at follow-up was significantly lower than in controls, these observations together suggests that abstainers had still not fully recovered to the level of the controls and that further GM volume recovery is likely with longer abstinence. We had previously observed large tissue volume increases in abstainers between 1 week and 8 months of abstinence (but essentially

Table 6
Change in internal and external negative strength in the four frontocerebellar subcircuits.

	Change Internal Negative Strength			
	DMN	ECN	SAL	SMN
Controls	0.221 (−0.173)	0.459 (−0.105)	0.192 (−0.185)	0.545 (−0.086)
Relapsers	0.181 (0.197)	0.761 (0.045)	0.094 (0.247)	0.274 (−0.161)
Abstainers	**0.012 (0.456)**	0.122 (0.290)	0.156 (0.259)	0.650 (0.083)
	Change External Negative Strength			
	DMN	**ECN**	**SAL**	**SMN**
Controls	0.166 (−0.196)	0.443 (−0.108)	0.069 (−0.257)	0.192 (−0.185)
Relapsers	0.248 (0.170)	0.162 (0.206)	*0.026 (0.327)*	0.107 (0.238)
Abstainers	0.460 (0.135)	0.394 (0.156)	0.140 (0.270)	0.334 (0.176)

p-values and corresponding effect sizes r (after Rosenthal, 1994) are given in parentheses; CON = controls, REL = relapsers, ABS = abstainers; DMN = default mode network subcircuit, ECN = executive-control network subcircuit, SAL = salience network subcircuit, SMN = sensorimotor network subcircuit. Significant p-values are highlighted in italic letters, the only p-value that survived a Bonferroni correction for 4 simultaneous corrections is highlighted in bold letters.

no recovery in relapsers), using another voxel-based analysis approach (deformation-based morphometry) that was sensitive to both GM and WM changes (Cardenas et al., 2007).

4.2. Effects of the AUD groups' global GM atrophy on the brain-wide GM network organization

In post-hoc analyses, we used a GTA approach to investigate if and how the locally restricted GM alterations detected by the VBM analysis in the two AUD groups interacted with the GM network organization of the entire brain. In combination with the PSI metric, the GTA measure of negative strength allows to measure diffuse atrophy as it quantifies with how many other brain regions a specific brain region shares the same atrophy profile. A high negative strength value indicates that a high number of other brain regions has a similar degree of atrophy as the brain region in question. We found that the brain-wide distribution pattern of negative strength of the two AUD groups at both timepoints was insofar similar to the controls as frontal, parietal, and occipital brain regions had in all three groups the highest and basal ganglia and sensorimotor cortex the lowest negative strength values. However, at both timepoints both AUD groups had globally higher negative strength values than the controls (Table 3), which indicates diffuse global GM atrophy in the two AUD groups relative to controls. The GTA thus made obvious and quantifiable what the results of the VBM analyses had allowed us to conclude only indirectly (by combining the GM findings for abstainers and controls at baseline and follow-up with the abstainers' GM increase during the three-months interval), the fact that both AUD groups showed persistent diffuse atrophy.

4.3. Internal and external effects of GM reduction on the network organization of the frontocerebellar circuit

The VBM had revealed significant AUD-related GM alterations in thalamus, frontal cortex and cerebellum, the three main constituent regions of the frontocerebellar circuit, in both AUD groups but no significant differences between them. To get a better understanding of such potential differences, we divided the frontocerebellar circuit into four subcircuits and used two modified versions of negative strength in their further characterizations.

Internal negative strength quantifies how homogeneous the degree of atrophy is between the brain regions belonging to the same subcircuit. Here again, a high internal negative strength value indicates that all regions of the same subcircuit show a similar degree of atrophy. The findings for internal negative strength of the four subcircuits mirrored closely those of the VBM, indicating a numerically lesser degree of local atrophy in all four subcircuits of the frontocerebellar circuit of abstainers than relapsers. Compared to controls, all four subcircuits in relapsers at baseline had significantly higher internal negative strength values than controls indicating atrophy across all subcircuits, whereas only the ECN- and DMN-subcircuits were atrophied in abstainers at baseline. At follow-up, internal negative strength of these two subcircuits in abstainers had recovered to such an extent that none of them did any longer differ significantly from controls, although only the degree of recovery of the DMN subcircuit in abstainers was significant. This finding was unexpected as one would assume that structural recovery of the ECN-subcircuit is an important prerequisite for successful abstinence (Wilcox et al., 2014). However, the DMN-subcircuit includes subcortical regions like the ventral tegmental area, and the bilateral nuclei accumbens and caudate that also belong to the core reward system (Alves et al., 2019), and structural recovery of these regions may promote successful recovery as well as recovery in linked brain regions subserving executive control. In contrast, relapsers did not show any significant recovery at all in internal negative strength of the four subcircuits except for the fact that the SAL-subcircuit had recovered to such a degree that its internal negative strength value was no longer significantly higher than that of the controls. We suggest that the absence of widespread internal structural recovery in relapsers is associated with the resumption of alcohol consumption during the observation interval, but that the diminished drinking during the scan interval (compared to the average lifetime drinking amounts before treatment, see Table 1) may be related to the improved internal structural integrity of the salience network observed at follow-up, potentially related to better functioning.

A subcircuit's mean external negative strength relates its atrophy to the degree of global atrophy of all other regions of the brain outside the subcircuit in question. A high external negative strength value indicates that the subcircuit's degree of atrophy is in the same range as the atrophy of the brain regions outside the subcircuit. The most important finding for external negative strength of the four subcircuits is that although both AUD groups had significantly higher external strength values than controls at both timepoints, only relapsers made a significant recovery. Their external negative strength in the SAL-subcircuit decreased over time, although the change did not survive our strict Bonferroni correction.

Assuming that the four subcircuits' internal and external negative strength values in healthy controls are representative of a GM network structure optimized to facilitate the interaction of these subcircuits, the selective internal and external negative strength recovery in relapsers with only the SAL-subcircuit having a GM network structure comparable to that of healthy controls, could also be interpreted to be problematic. Functionally, the fine-tuned interaction between the ECN-, DMN-, and particularly SAL-subcircuits is important for switching from an unconstrained state during rest to a task-focused state vital for goal-directed behavior (Goulden et al., 2014; Menon and Uddin, 2010; Seeley et al., 2007; Sridharan et al., 2008). An impairment of these three subcircuits is a characteristic finding of task-induced fMRI studies in AUD patients (Zhang and Volkow, 2019; Zilverstand et al., 2018), and the selective GM recovery of only one of the three subcircuits in relapsers may reflect an imbalance in the fine-tuned functional interaction between the subcircuits potentially associated with maladaptive alcohol use behavior as seen in the relapsers.

5. Limitations

One limitation of the study is the relatively small size of the abstainer sample, which did not allow to control for sex and smoking status in addition to TIV and age. However, TIV has been described as a more important variable determining GM volume than sex (Lüders et al., 2002; Brun et al., 2009; Jäncke et al., 2015). While the small number of smokers among the controls (3/25) and abstainers (2/15) may not have much of an effect on the VBM results, the higher smoker fraction in the relapsers (9/23) may have influenced our findings. However, in follow-up tests with even the most lenient threshold of $p < 0.001$ uncorrected, we were unable to detect smoking effects among the relapsers; we are therefore confident that the extensive GM reduction observed in relapsers was not driven by the higher number of smokers in this group.

6. Conclusion

VBM and post-hoc GM network analyses confirmed our hypothesis that group-specific differences of AUD-related GM reduction and change in the frontocerebellar circuit early in treatment can inform about future treatment success. Relative to healthy controls, relapsers presented with significant and persistent GM reductions in all main regions of the frontocerebellar circuit at both one month and four months after alcohol cessation. By contrast, abstainers, who at baseline showed the most pronounced GM reduction in the thalamus while the other core regions of the frontocerebellar circuit (frontal cortex and cerebellum) were spared, showed a significant GM increase encompassing the entire frontocerebellar circuit, far beyond the brain regions that had originally shown GM atrophy. These widespread volumetric improvements in abstainers and their general absence in relapsers suggest that productive

structural plasticity in the frontocerebellar circuit supports successful abstinence in AUD.

The post-hoc GTAs were more sensitive than the voxel-based structural analyses for understanding AUD-related GM reduction since they were able to reveal and quantify a persistent diffuse global atrophy in both AUD groups relative to controls at follow-up. However, the most important GTA finding was that abstainers and relapsers differed in the degree the four subcircuits recovered during the three-months interval. The internal negative strength of all four subcircuits in abstainers recovered to such a degree that they were no longer significantly different from healthy controls, with the DMN-subcircuit recovering most significantly. In contrast, relapsers who had not shown any significant GM recovery in the VBM analyses, presented with a normal (i.e., not anymore significantly increased relative) external negative strength value at follow-up only in the SAL-subcircuit. These distinctly different recovery patterns in the two AUD groups could suggest that relapsers do not just present with a more severe expression of the same AUD consequences than abstainers, but that AUD affects the four subcircuits differently in relapsers and abstainers with defining consequences for treatment success.

CRediT authorship contribution statement

Angela M. Muller: Conceptualization, Formal analysis, Methodology, Visualization, Writing – original draft, Writing – review & editing. **Dieter J. Meyerhoff:** Conceptualization, Funding acquisition, Resources, Supervision, Writing – review & editing.

Declaration of Competing Interest

The authors declare that they have no known competing financial interests or personal relationships that could have appeared to influence the work reported in this paper.

Acknowledgements

This work was supported by NIH AA010788, DA039903, and DoD W81XWH-15-2-0020 (all to DJM) and by San Francisco VA Medical Center resources. The research was administered by the Northern California Institute for Research and Education. The funding and administrative agencies had no role in the design of the study, the collection and analysis of data or the decision to publish. In particular, the authors would like to thank Dr. Susanne G. Mueller for providing the MATLAB codes for the calculation of the PSI matrices. We extend our appreciation to all who volunteered for this research. For critical help with participant recruitment, we thank the substance abuse treatment personnel at the San Francisco VA as well as Dr. David Pating and his team at Kaiser Permanente San Francisco. We also wish to thank Thomas Schmidt, Randi Brown, and Rachel Gonzalez for participant recruitment and assessment as well as Alen Tersakyan for MR data acquisition.

Data Availability Statement

Restrictions apply to the datasets: the datasets for this manuscript are not publicly available because they were created as part of Veteran's Administration approved research. Requests to access the datasets should be directed to the senior author.

Appendix A. Supplementary data

Supplementary data to this article can be found online at https://doi.org/10.1016/j.nicl.2021.102788.

References

Alves, P.N., Foulon, C., Karolis, V., Bzdok, D., Margulies, D.S., Volle, E., Thiebaut de Schotten, M., 2019. An improved neuroanatomical model of the default-mode network reconciles previous neuroimaging and neuropathological findings. Commun. Biol. 2, 370. https://doi.org/10.1038/s42003-019-0611-3.

Bach, P., Koopmann, A., Bumb, J.M., Vollstädt-Klein, S., Reinhard, I., Rietschel, M., Witt, S.H., Wiedemann, K., Kiefer, F., 2020. Leptin predicts cortical and subcortical gray matter volume recovery in alcohol dependent patients: A longitudinal structural magnetic resonance imaging study. Horm. Behav. 124, 104749. https://doi.org/10.1016/j.yhbeh.2020.104749.

Beck, A.T., Ward, C.H., Mendelson, M., Mock, J., Erbaugh, J., 1961. An inventory for measuring depression. Arch. Gen. Psychiatry 4, 561–571. https://doi.org/10.1001/archpsyc.1961.01710120031004.

Brun, C.C., Leporé, N., Luders, E., Chou, Y.Y., Madsen, S.K., Toga, A.W., Thompson, P.M., 2009. Sex differences in brain structure in auditory and cingulate regions. NeuroReport 20 (10), 930–935. https://doi.org/10.1097/wnr.0b013e32832c5e65.

Buckner, R.L., Krienen, F.M., Castellanos, A., Diaz, J.C., Yeo, B.T., 2011. The organization of the human cerebellum estimated by intrinsic functional connectivity. J. Neurophysiol. 106 (5), 2322–2345. https://doi.org/10.1152/jn.00339.2011.

Cardenas, V.A., Studholme, C., Gazdzinski, S., Durazzo, T.C., Meyerhoff, D.J., 2007. Deformation-based morphometry of brain changes in alcohol dependence and abstinence. NeuroImage 34 (3), 879–887. https://doi.org/10.1016/j.neuroimage.2006.10.015.

Cauda, F., Mancuso, L., Nani, A., Ficco, L., Premi, E., Manuello, J., Liloia, D., Gelmini, G., Duca, S., Costa, T., 2020. Hubs of long-distance co-alteration characterize brain pathology. Hum. Brain Mapp. 41 (14), 3878–3899. https://doi.org/10.1002/hbm.25093.

Chanraud-Guillermo, S., Andoh, J., Martelli, C., Artiges, E., Pallier, C., Aubin, H.J., Martinot, J.L., Reynaud, M., 2009. Imaging of language-related brain regions in detoxified alcoholics. Alcohol. Clin. Exp. Res. 33 (6), 977–984. https://doi.org/10.1111/j.1530-0277.2009.00918.x.

Chanraud, S., Martelli, C., Delain, F., Kostogianni, N., Douaud, G., Aubin, H.J., Reynaud, M., Martinot, J.L., 2007. Brain morphometry and cognitive performance in detoxified alcohol-dependents with preserved psychosocial functioning. Neuropsychopharmacology : Off. Publ. Am. College Neuropsychopharmacol. 32 (2), 429–438. https://doi.org/10.1038/sj.npp.1301219.

Chye, Y., Mackey, S., Gutman, B.A., Ching, C.R.K., Batalla, A., Blaine, S., Brooks, S., Caparelli, E.C., Cousijn, J., Dagher, A., Foxe, J.J., Goudriaan, A.E., Hester, R., Hutchison, K., Jahanshad, N., Kaag, A.M., Korucuoglu, O., Li, C.-S., London, E.D., Lorenzetti, V., Luijten, M., Martin-Santos, R., Meda, S.A., Momenan, R., Morales, A., Orr, C., Paulus, M.P., Pearlson, G., Reneman, L., Schmaal, L., Sinha, R., Solowij, N., Stein, D.J., Stein, E.A., Tang, D., Uhlmann, A., Holst, R., Veltman, D.J., Verdejo-Garcia, A., Wiers, R.W., Yücel, M., Thompson, P.M., Conrod, P., Garavan, H., 2020. Subcortical surface morphometry in substance dependence: An ENIGMA addiction working group study. Addict. Biol. 25 (6) https://doi.org/10.1111/adb.12830.

Demirakca, T., Ende, G., Kämmerer, N., Welzel-Marquez, H., Hermann, D., Heinz, A., Mann, K., 2011. Effects of alcoholism and continued abstinence on brain volumes in both genders. Alcohol. Clin. Exp. Res. 35 (9), 1678–1685. https://doi.org/10.1111/j.1530-0277.2011.01514.x.

Durazzo, T.C., Meyerhoff, D.J., 2020 Oct. Changes of frontal cortical subregion volumes in alcohol dependent individuals during early abstinence: associations with treatment outcome. Brain Imaging Behav. 14 (5), 1588–1599. https://doi.org/10.1007/s11682-019-00089-5.

Durazzo, T.C., Mon, A., Gazdzinski, S., Meyerhoff, D.J., 2017. Regional brain volume changes in alcohol-dependent individuals during early abstinence: associations with relapse following treatment. Addict. Biol. 22 (5), 1416–1425. https://doi.org/10.1111/adb.12420.

Garrett, D.D., Epp, S.M., Perry, A., Lindenberger, U., 2018. Local temporal variability reflects functional integration in the human brain. NeuroImage 183, 776–787. https://doi.org/10.1016/j.neuroimage.2018.08.019.

Gazdzinski, S., Durazzo, T.C., Meyerhoff, D.J., 2005. Temporal dynamics and determinants of whole brain tissue volume changes during recovery from alcohol dependence. Drug Alcohol Depend. 78 (3), 263–273. https://doi.org/10.1016/j.drugalcdep.2004.11.004.

Goulden, N., Khusnulina, A., Davis, N.J., Bracewell, R.M., Bokde, A.L., McNulty, J.P., Mullins, P.G., 2014. The salience network is responsible for switching between the default mode network and the central executive network: replication from DCM. NeuroImage 99, 180–190. https://doi.org/10.1016/j.neuroimage.2014.05.052.

Grodin, E.N., Lin, H., Durkee, C.A., Hommer, D.W., Momenan, R., 2013. Deficits in cortical, diencephalic and midbrain gray matter in alcoholism measured by VBM: Effects of co-morbid substance abuse. NeuroImage. Clinical 2, 469–476. https://doi.org/10.1016/j.nicl.2013.03.013.

Habas, C., Manto, M., Cabaraux, P., 2019. The Cerebellar Thalamus. Cerebellum (London, England) 18 (3), 635–648. https://doi.org/10.1007/s12311-019-01019-3.

Habas, C., Kamdar, N., Nguyen, D., Prater, K., Beckmann, C.F., Menon, V., Greicius, M. D., 2009. Distinct cerebellar contributions to intrinsic connectivity networks. J. Neurosci. : Off. J. Soc. Neurosci. 29 (26), 8586–8594. https://doi.org/10.1523/JNEUROSCI.1868-09.2009.

Halassa, M.M., Sherman, S.M., 2019. Thalamocortical Circuit Motifs: A General Framework. Neuron 103 (5), 762–770. https://doi.org/10.1016/j.neuron.2019.06.005.

Hoffstaedter, F., Grefkes, C., Roski, C., Caspers, S., Zilles, K., Eickhoff, S.B., 2015. Age-related decrease of functional connectivity additional to gray matter atrophy in a network for movement initiation. Brain Struct. Funct. 220 (2), 999–1012. https://doi-org.ucsf.idm.oclc.org/10.1007/s00429-013-0696-2.

Hwang, K., Bertolero, M.A., Liu, W.B., D'Esposito, M., 2017. The Human Thalamus Is an Integrative Hub for Functional Brain Networks. J. Neurosci. : Official J. Soc. Neurosci. 37 (23), 5594–5607. https://doi.org/10.1523/JNEUROSCI.0067-17.2017.
Jäncke, L., Mérillat, S., Liem, F., Hänggi, J., 2015. Brain size, sex, and the aging brain. Hum. Brain Mapp. 36 (1), 150–169. https://doi.org/10.1002/hbm.22619.
Joliot, M., Jobard, G., Naveau, M., Delcroix, N., Petit, L., Zago, L., Crivello, F., Mellet, E., Mazoyer, B., Tzourio-Mazoyer, N., 2015. AICHA: An atlas of intrinsic connectivity of homotopic areas. J. Neurosci. Methods 254, 46–59. https://doi.org/10.1016/j.jneumeth.2015.07.013.
Keifer Jr, O.P., Hurt, R.C., Gutman, D.A., Keilholz, S.D., Gourley, S.L., Ressler, K.J., 2015. Voxel-based morphometry predicts shifts in dendritic spine density and morphology with auditory fear conditioning. Nat. Commun. 6, 7582. https://doi.org/10.1038/ncomms8582.
Krienen, F.M., Buckner, R.L., 2009. Segregated fronto-cerebellar circuits revealed by intrinsic functional connectivity. Cerebral cortex (New York, N.Y. : 1991) 19 (10), 2485–2497. https://doi.org/10.1093/cercor/bhp135.
Le Berre, A.P., Pitel, A.L., Chanraud, S., Beaunieux, H., Eustache, F., Martinot, J.L., Reynaud, M., Martelli, C., Rohlfing, T., Sullivan, E.V., Pfefferbaum, A., 2014. Chronic alcohol consumption and its effect on nodes of frontocerebellar and limbic circuitry: comparison of effects in France and the United States. Hum. Brain Mapp. 35 (9), 4635–4653. https://doi.org/10.1002/hbm.22500.
Li, J., Wang, Y., Xu, Z., Liu, T., Zang, X., Li, M., Ma, L., 2019. Whole-brain morphometric studies in alcohol addicts by voxel-based morphometry. Ann. Translat. Med. 7 (22), 635. https://doi.org/10.21037/atm.2019.10.90.
Liloia, D., Mancuso, L., Uddin, L.Q., Costa, T., Nani, A., Keller, R., Manuello, J., Duca, S., Cauda, F., 2021. Gray matter abnormalities follow non-random patterns of co-alteration in autism: Meta-connectomic evidence. NeuroImage. Clinical 30, 102583. https://doi.org/10.1016/j.nicl.2021.102583.
Lüders, E., Steinmetz, H., Jäncke, L., 2002. Brain size and grey matter volume in the healthy human brain. NeuroReport 13 (17), 2371–2374. https://doi.org/10.1097/01.wnr.0000049603.85580.da.
Mackey, S., Allgaier, N., Chaarani, B., Spechler, P., Orr, C., Bunn, J., Allen, N.B., Alia-Klein, N., Batalla, A., Blaine, S., Brooks, S., Caparelli, E., Chye, Y.Y., Cousijn, J., Dagher, A., Desrivieres, S., Feldstein-Ewing, S., Foxe, J.J., Goldstein, R.Z., Goudriaan, A.E., Heitzeg, M.M., Hester, R., Hutchison, K., Korucuoglu, O., Li, C.-S., London, E., Lorenzetti, V., Luijten, M., Martin-Santos, R., May, A., Momenan, R., Morales, A., Paulus, M.P., Pearlson, G., Rousseau, M.-E., Salmeron, B.J., Schluter, R., Schmaal, L., Schumann, G., Sjoerds, Z., Stein, D.J., Stein, E.A., Sinha, R., Solowij, N., Tapert, S., Uhlmann, A., Veltman, D., van Holst, R., Whittle, S., Wiers, R., Wright, M. J., Yücel, M., Zhang, S., Yurgelun-Todd, D., Hibar, D.P., Jahanshad, N., Evans, A., Thompson, P.M., Glahn, D.C., Conrod, P., Garavan, H., 2019. Mega-Analysis of Gray Matter Volume in Substance Dependence: General and Substance-Specific Regional Effects. Am. J. Psychiatry 176 (2), 119–128. https://doi.org/10.1176/appi.ajp.2018.17040415.
Malone, I.B., Leung, K.K., Clegg, S., Barnes, J., Whitwell, J.L., Ashburner, J., Fox, N.C., Ridgway, G.R., 2015. Accurate automatic estimation of total intracranial volume: a nuisance variable with less nuisance. NeuroImage 104, 366–372. https://doi.org/10.1016/j.neuroimage.2014.09.034.
Mechtcheriakov, S., Brenneis, C., Egger, K., Koppelstaetter, F., Schocke, M., Marksteiner, J., 2007. A widespread distinct pattern of cerebral atrophy in patients with alcohol addiction revealed by voxel-based morphometry. J. Neurol. Neurosurg. Psychiatry 78 (6), 610–614. https://doi.org/10.1136/jnnp.2006.095869.
Menon, V., Uddin, L.Q., 2010. Saliency, switching, attention and control: a network model of insula function. Brain Struct. Funct. 214 (5–6), 655–667. https://doi.org/10.1007/s00429-010-0262-0.
Meyerhoff, D.J., Durazzo, T.C., 2020. Modelling neurocognitive and neurobiological recovery in addiction. In: Verdejo-Garcia, A. (Ed.), Cognition and addiction. A researcher's guide from mechanisms toward interventions, 1st ed. Academic Press, Cambridge, MA, pp. 379–386.
Mueller, S.G., Meyerhoff, D.J., 2021. The gray matter structural connectome and its relationship to alcohol relapse: Reconnecting for recovery. Addict. Biol. 26 (1), e12860. https://doi.org/10.1111/adb.12860.
Mueller, S.G., Weiner, M.W., 2017. Amyloid Associated Intermittent Network Disruptions in Cognitively Intact Older Subjects: Structural Connectivity Matters. Front. Aging Neurosci. 9, 418. https://doi-org.ucsf.idm.oclc.org/10.3389/fnagi.2017.00418.
Mueller, S.G., Bateman, L.M., Laxer, K.D., 2014. Evidence for brainstem network disruption in temporal lobe epilepsy and sudden unexplained death in epilepsy. NeuroImage. Clinical 5, 208–216. https://doi.org/10.1016/j.nicl.2014.06.0.
Müller, E.J., Munn, B., Hearne, L.J., Smith, J.B., Fulcher, B., Arnatkevičiūtė, A., Lurie, D. J., Cocchi, L., Shine, J.M., 2020. Core and matrix thalamic sub-populations relate to spatio-temporal cortical connectivity gradients. NeuroImage 222, 117224. https://doi.org/10.1016/j.neuroimage.2020.117224.
Muller, A.M., Meyerhoff, D.J., 2021. Maladaptive brain organization at 1 month into abstinence as an indicator for future relapse in patients with alcohol use disorder. Eur. J. Neurosci. 53 (8), 2923–2938. https://doi.org/10.1111/ejn.15161.
Navarri, X., Afzali, M.H., Lavoie, J., Sinha, R., Stein, D.J., Momenan, R., Veltman, D.J., Korucuoglu, O., Sjoerds, Z., van Holst, R.J., Hester, R., Orr, C., Cousijn, J., Yucel, M., Lorenzetti, V., Wiers, R., Jahanshad, N., Glahn, D.C., Thompson, P.M., Mackey, S., et al., 2020. How do substance use disorders compare to other psychiatric conditions on structural brain abnormalities? A cross-disorder meta-analytic comparison using the ENIGMA consortium findings. Human Brain Mapping. https://doi.org/10.1002/hbm.2511410.1002/hbm.25114. Advance online publication.
Pandey, A.K., Ardekani, B.A., Kamarajan, C., Zhang, J., Chorlian, D.B., Byrne, K.-H., Pandey, G., Meyers, J.L., Kinreich, S., Stimus, A., Porjesz, B., 2018. Lower prefrontal and hippocampal volume and diffusion tensor imaging differences reflect structural and functional abnormalities in abstinent individuals with alcohol use disorder. Alcohol. Clin. Exp. Res. 42 (10), 1883–1896. https://doi.org/10.1111/acer.13854.
Patton, J.H., Stanford, M.S., Barratt, E.S., 1995. Factor structure of the Barratt impulsiveness scale. J. Clin. Psychol. 51 (6), 768–774. https://doi.org/10.1002/1097-4679(199511)51:6<768::aid-jclp2270510607>3.0.co;2-1.
Pergola, G., Danet, L., Pitel, A.L., Carlesimo, G.A., Segobin, S., Pariente, J., Suchan, B., Mitchell, A.S., Barbeau, E.J., 2018. The Regulatory Role of the Human Mediodorsal Thalamus. Trends Cognitive Sci. 22 (11), 1011–1025. https://doi.org/10.1016/j.tics.2018.08.006.
Pitel, A.L., Segobin, S.H., Ritz, L., Eustache, F., Beaunieux, H., 2015. Thalamic abnormalities are a cardinal feature of alcohol-related brain dysfunction. Neurosci. Biobehav. Rev. 54, 38–45. https://doi.org/10.1016/j.neubiorev.2014.07.023.
Reinert, D.F., Allen, J.P., 2002. The Alcohol Use Disorders Identification Test (AUDIT): a review of recent research. Alcohol. Clin. Exp. Res. 26 (2), 272–279.
Ritz, L., Segobin, S., Lannuzel, C., Boudehent, C., Vabret, F., Eustache, F., Beaunieux, H., Pitel, A.L., 2016. Direct voxel-based comparisons between grey matter shrinkage and glucose hypometabolism in chronic alcoholism. J. Cerebral Blood Flow Metabol. : Off. J. Int. Soc. Cerebral Blood Flow Metabol. 36 (9), 1625–1640. https://doi.org/10.1177/0271678X15611136.
Rosenthal, R., 1994. Parametric measures of effect size. In: Cooper, H., Hedges, L.V. (Eds.), The Handbook of Research Synthesis. Russell Sage Foundation, New York, NY, pp. 231–244.
Rubinov, M., Sporns, O., 2010. Complex network measures of brain connectivity: uses and interpretations. NeuroImage 52 (3), 1059–1069. https://doi.org/10.1016/j.neuroimage.2009.10.003.
Salimi-Khorshidi, G., Smith, S.M., Nichols, T.E., 2009. Adjusting the neuroimaging statistical inferences for nonstationarity. Medical Image Computing and Computer-assisted Intervention : MICCAI International Conference on Medical Image Computing and Computer-Assisted Intervention 12 (Pt 1), 992–999. https://doi.org/10.1007/978-3-642-04268-3_122.
Segobin, S., Laniepce, A., Ritz, L., Lannuzel, C., Boudehent, C., Cabé, N., Urso, L., Vabret, F., Eustache, F., Beaunieux, H., Pitel, A.L., 2019. Dissociating thalamic alterations in alcohol use disorder defines specificity of Korsakoff's syndrome. Brain : J. Neurol. 142 (5), 1458–1470. https://doi.org/10.1093/brain/awz056.
Segobin, S.H., Chételat, G., Le Berre, A.-P., Lannuzel, C., Boudehent, C., Vabret, F., Eustache, F., Beaunieux, H., Pitel, A.-L., 2014. Relationship between brain volumetric changes and interim drinking at six months in alcohol-dependent patients. Alcohol. Clin. Exp. Res. 38 (3), 739–748. https://doi.org/10.1111/acer.12300.
Seeley, W.W., Crawford, R.K., Zhou, J., Miller, B.L., Greicius, M.D., 2009. Neurodegenerative diseases target large-scale human brain networks. Neuron 62 (1), 42–52. https://doi.org/10.1016/j.neuron.2009.03.024.
Seeley, W.W., Menon, V., Schatzberg, A.F., Keller, J., Glover, G.H., Kenna, H., Reiss, A.L., Greicius, M.D., 2007. Dissociable intrinsic connectivity networks for salience processing and executive control. J. Neurosci. : Off. J. Soc. Neurosci. 27 (9), 2349–2356. https://doi.org/10.1523/JNEUROSCI.5587-06.2007.
Shafiei, G., Markello, R.D., Makowski, C., Talpalaru, A., Kirschner, M., Devenyi, G.A., Guma, E., Hagmann, P., Cashman, N.R., Lepage, M., Chakravarty, M.M., Dagher, A., Mišić, B., 2020. Spatial Patterning of Tissue Volume Loss in Schizophrenia Reflects Brain Network Architecture. Biol. Psychiatry 87 (8), 727–735. https://doi-org.ucsf.idm.oclc.org/10.1016/j.biopsych.2019.09.031.
Sherman, S.M., 2017. Functioning of Circuits Connecting Thalamus and Cortex. Comprehens. Physiol. 7 (2), 713–739. https://doi.org/10.1002/cphy.c160032.
Sherman, S.M., 2016. Thalamus plays a central role in ongoing cortical functioning. Nat. Neurosci. 19 (4), 533–541. https://doi.org/10.1038/nn.4269.
Sherman, S.M., 2007. The thalamus is more than just a relay. Curr. Opin. Neurobiol. 17 (4), 417–422. https://doi.org/10.1016/j.conb.2007.07.003.
Smith, S.M., Nichols, T.E., 2009. Threshold-free cluster enhancement: addressing problems of smoothing, threshold dependence and localisation in cluster inference. NeuroImage 44 (1), 83–98. https://doi.org/10.1016/j.neuroimage.2008.03.061.
Spielberger, C.D., Vagg, P.R., 1984. Psychometric properties of the STAI: a reply to Ramanaiah, Franzen, and Schill. J. Pers. Assess. 48 (1), 95–97. https://doi.org/10.1207/s15327752jpa4801_16.
Sridharan, D., Levitin, D.J., Menon, V., 2008. A critical role for the right fronto-insular cortex in switching between central-executive and default-mode networks. PNAS 105 (34), 12569–12574. https://doi.org/10.1073/pnas.0800005105.
Sullivan, E.V., Pfefferbaum, A., 2005. Neurocircuitry in alcoholism: a substrate of disruption and repair. Psychopharmacology 180 (4), 583–594. https://doi.org/10.1007/s00213-005-2267-6.
Sullivan, E.V., Harding, A.J., Pentney, R., Dlugos, C., Martin, P.R., Parks, M.H., Desmond, J.E., Chen, S.H., Pryor, M.R., De Rosa, E., Pfefferbaum, A., 2003. Disruption of frontocerebellar circuitry and function in alcoholism. Alcohol. Clin. Exp. Res. 27 (2), 301–309. https://doi.org/10.1097/01.ALC.0000052584.05305.98.
Thayer, R.E., Hagerty, S.L., Sabbineni, A., Claus, E.D., Hutchison, K.E., Weiland, B.J., 2016. Negative and interactive effects of sex, aging, and alcohol abuse on gray matter morphometry. Hum. Brain Mapp. 37 (6), 2276–2292. https://doi.org/10.1002/hbm.23172.
Tzourio-Mazoyer, N., Landeau, B., Papathanassiou, D., Crivello, F., Etard, O., Delcroix, N., Mazoyer, B., Joliot, M., 2002. Automated anatomical labeling of activations in SPM using a macroscopic anatomical parcellation of the MNI MRI single-subject brain. NeuroImage 15 (1), 273–289. https://doi.org/10.1006/nimg.2001.0978.
Usrey, W.M., Sherman, S.M., 2019. Corticofugal circuits: Communication lines from the cortex to the rest of the brain. J. Comp. Neurol. 527 (3), 640–650. https://doi.org/10.1002/cne.24423.

van Eijk, J., Demirakca, T., Frischknecht, U., Hermann, D., Mann, K., Ende, G., 2013. Rapid partial regeneration of brain volume during the first 14 days of abstinence from alcohol. Alcohol. Clin. Exp. Res. 37 (1), 67–74. https://doi.org/10.1111/j.1530-0277.2012.01853.x.

Wig, G.S., 2017. Segregated Systems of Human Brain Networks. Trends Cognitive Sci. 21 (12), 981–996. https://doi.org/10.1016/j.tics.2017.09.006.

Wilcox, C.E., Dekonenko, C.J., Mayer, A.R., Bogenschutz, M.P., Turner, J.A., 2014. Cognitive control in alcohol use disorder: deficits and clinical relevance. Rev. Neurosci. 25 (1), 1–24. https://doi.org/10.1515/revneuro-2013-0054.

Xiao, P., Dai, Z., Zhong, J., Zhu, Y., Shi, H., Pan, P., 2015. Regional gray matter deficits in alcohol dependence: A meta-analysis of voxel-based morphometry studies. Drug Alcohol. Depend. 153, 22–28. https://doi.org/10.1016/j.drugalcdep.2015.05.030.

Yang, X., Tian, F., Zhang, H., Zeng, J., Chen, T., Wang, S., Jia, Z., Gong, Q., 2016. Cortical and subcortical gray matter shrinkage in alcohol-use disorders: a voxel-based meta-analysis. Neurosci. Biobehav. Rev. 66, 92–103. https://doi.org/10.1016/j.neubiorev.2016.03.034.

Zahr, N.M., Pfefferbaum, A., Sullivan, E.V., 2017. Perspectives on fronto-fugal circuitry from human imaging of alcohol use disorders. Neuropharmacology 122, 189–200. https://doi.org/10.1016/j.neuropharm.2017.01.018.

Zahr, N.M., Pitel, A.L., Chanraud, S., Sullivan, E.V., 2010. Contributions of studies on alcohol use disorders to understanding cerebellar function. Neuropsychol. Rev. 20 (3), 280–289. https://doi.org/10.1007/s11065-010-9141-y.

Zhang, R., Volkow, N.D., 2019. Brain default-mode network dysfunction in addiction. NeuroImage 200, 313–331. https://doi.org/10.1016/j.neuroimage.2019.06.036.

Zhang, D., Snyder, A.Z., Fox, M.D., Sansbury, M.W., Shimony, J.S., Raichle, M.E., 2008. Intrinsic functional relations between human cerebral cortex and thalamus. J. Neurophysiol. 100 (4), 1740–1748. https://doi.org/10.1152/jn.90463.2008.

Zilverstand, A., Huang, A.S., Alia-Klein, N., Goldstein, R.Z., 2018. Neuroimaging Impaired Response Inhibition and Salience Attribution in Human Drug Addiction: A Systematic Review. Neuron 98 (5), 886–903. https://doi.org/10.1016/j.neuron.2018.03.048.

Zou, X., Durazzo, T.C., Meyerhoff, D.J., 2018. Regional Brain Volume Changes in Alcohol-Dependent Individuals During Short-Term and Long-Term Abstinence. Alcohol. Clin. Exp. Res. 42 (6), 1062–1072. https://doi.org/10.1111/acer.13757.